Earth's radiation belts ions: patterns of the spatial-energy structure and its solar-cyclic variations

Alexander S. Kovtyukh
Skobeltsyn Institute of Nuclear Physics, Moscow State University, Moscow, 119234, Russia; kovtyukhas@mail.ru

Abstract Spatial-energy distributions of the stationary fluxes of protons, helium ~~ions~~ and ions of carbon-nitrogen-oxygen (CNO) group, with energy from $E \sim 100$ keV to 200 MeV, in the Earth's radiation belts (ERB), at $L \sim 1$–8, are considered here ~~by the~~ using data ~~of the~~ from satellites ~~for~~ in the period 1961–2017. It ~~is find~~ has been found that the results of these measurements line up in the space $\{E, L\}$ ~~by~~ following some regular patterns. Solar-cyclic (11-year) variations in the distributions of protons, helium ~~ions~~ and CNO group ions fluxes in the ERB are studied. It has been observed that in the inner regions of the ERB, ~~the ions~~ ion fluxes decrease with increasing solar activity~~. It is find~~ and that the solar-cyclic variations of fluxes ~~for ions with~~ of $Z \geq 2$ ions are much greater than for protons; moreover, it seems that they ~~and~~ increase with increasing ~~an~~ atomic number Z ~~of the ions~~. ~~The~~ Finally, the possible physical mechanisms leading to formation of this spatial-energy structure and to the solar-cyclic variations of the ERB ion fluxes are discussed.

Keywords. Magnetospheric physics (energetic particles, trapped). Radiation belts.

1 Introduction

~~The Earth's radiation belts (ERB)~~ The ERB consist mainly of charged particles with energy from E ~ 100 keV to several hundreds of megaelectronvolt (MeV). These particles are trapped by the geomagnetic field at altitudes from ~ 200 kilometers to ~ 50–70 thousands kilometers. The ERB is consisted mainly from electrons and protons. In ~~the~~ ERB there are also ~~ions of~~ helium nuclei and other Z >2 ions (like oxygen etc), ~~oxygen, and other elements with the atomic number $Z \geq 2$,~~ where Z is the charge of the atomic nucleus with respect to the charge of the proton. During geomagnetic disturbances, ion fluxes, and ~~its~~ their distributions are ~~varied~~ changed. These fluxes depend also on the phase of the solar cycle, conditions in the interplanetary space, and other factors.

Particles with different energy E and pitch angles α (α is the angle between ~~a~~ the local vector of the magnetic field and the vector of a particle velocity), which are injected into some point of the geomagnetic trap, ~~are~~ drifted ~~with~~ conserving the adiabatic invariants (μ, K, Φ) and populate a narrow layer surrounding the Earth (Alfvén and Fälthammar, 1963; Northrop, 1963). This layer called the drift shell. Therefore, experimental data on the ERB ~~do most simply~~ are often represented in coordinates $\{L, B\}$, where L is ~~parameter of a drift shell~~ the drift shell parameter and B is ~~a~~ the local induction of the magnetic field (McIlwain, 1961). For the dipole magnetic field L is a distance, in the equatorial plane, from the given magnetic field line to the center of the dipole itself (in ~~the~~ Earth's radii R_E).

The stationary fluxes J of the ERB particles with given energy and pitch angle α ~~are~~ decrease~~d~~ usually when the point of observation is shifted from the equatorial plane to ~~a~~ higher latitudes along certain magnetic field line (if we exclude the peripheral regions of the geomagnetic trap, where the drift shells of the captured particles are split and branched). This dependence of the particle fluxes is described by the functions $J(B/B_0)$, were B and B_0 are values of the magnetic field at the point of observation and in the equatorial plane on the same magnetic field line respectively.

Outer and inner regions of the ERB are maintained in ~~the~~ dynamic equilibrium with the environment by ~~the~~ different mechanisms (see review Kovtyukh, 2018).

The outer belt ($L > 3.5$) ~~of ions~~ is formed mainly by the mechanisms of ~~the~~ radial diffusion of ~~these~~ such ions ~~to~~ towards the Earth under the action of fluctuations of ~~an~~ both electric and magnetic fields resonating with ~~a~~ their drift periods ~~of these ions~~. This transport is accompanied by the betatron acceleration ~~of ions~~ and by the ionization losses of the ions ~~in~~ as a result of their interactions with the plasmasphere and with residual atmosphere.

The inner belt ($L < 2.5$) of protons with $E > 10$ MeV ~~is~~ was formed mainly as a result of decay of neutrons knocked from the nuclei of the atmospheric atoms by the Galactic Cosmic Rays ~~(GCR)~~. For protons with $E < 10$ MeV this mechanism (CRAND) is supplemented by the radial diffusion of particles from the outer to the inner belt. The inner belt of ions with $Z > 4$ was formed mainly from the ions of the Anomalous component of Cosmic Rays ~~(ACR)~~.

In the intermediate region ($2.5 < L < 3.5$) is operated also the mechanism of ~~a~~ ion capture ~~of the ions~~ from ~~the~~ Solar Cosmic Rays ~~(SCR)~~ takes place during strong magnetic storms (see, e.g., Selesnick et al., 2014).

Thus, the main mechanisms of formation of the ERB, together with the sources of injection and losses of ~~the~~ ions, are known. However, for ~~the~~ comprehensive verification of the physical models and to ~~identification~~ identify ~~of~~ the mathematical models and their parameters, the formulation of ~~sufficiently~~ complete and reliable empirical models of the ERB for each of the ion components, ~~it~~ is necessary; it is also necessary ~~also~~ for ensuring the safety of space flights.

These models can be created only ~~on a basis of the~~ using experimental data, ~~are~~ obtained over many years and decades; such models (see, e.g., Ginet et al., 2013) were already created for protons (AP8/AP9)~~. These models~~ and they are widely used in ~~the~~ space research. ~~However,~~ On the contrary, measurements of ~~fluxes of the ions with~~ $Z \geq 2$ ion fluxes ~~are represented a difficult~~

suffer from technical problems due to ~~a~~ small ~~fluxes of these ions~~ statistics and high background ~~fluxes~~ of protons and electrons. ~~The~~ For this reasons, empirical and semi-empirical models ~~of the ERB developed~~ for ~~ions with~~ $Z \geq 2$ ions, are applicable only to very limited regions of the space $\{E, L\}$.

~~There are problems connected with limited and incomplete information on the fluxes of ions with $Z \geq 2$ in the ERB, especially in the energy range from tens to hundreds of megaelectronvolt.~~ One of the main problems of this work is to consider the possibility to create a sufficiently complete and reliable empirical models of the ERB for these ions based on currently available experimental data.

In the following sections, ~~are considered~~ the spatial-energy structure of the ERB in the spaces $\{E, L\}$ for protons, helium ~~ions~~ and ~~of the~~ CNO group ions on the experimental data (Sect. 2) together with the possible physical mechanisms of formation of these structures and its solar-cyclic variations (Sect. 3) are ~~discussed~~ considered, and the main conclusions of this work are given (Sect. 4).

2 Spatial-energy distributions of the ion fluxes near the equatorial plane

There can be ions trapped ~~on the~~ in drift shells only ~~ions~~ with energies less than some maximum values, determined by the Alfvén's criterion: $\rho_i(L, E, M_i, Q_i) << R_c(L)$, where ρ_i is the ~~gyroradii~~ gyroradius of ions, and R_c is the radius of curvature of the magnetic field near the equatorial plane (M_i and Q_i are mass and charge of ions with respect to the corresponding values for protons). According to this criterion and the theory of stochastic motion of particles, the geomagnetic trap can capture and durably hold only ions with E (MeV) $< 2000 \times (Q_i^2/M_i)\, L^{-4}$ (Ilyin et al., 1984). The green line in Figs 1-6 ~~is present~~ represents this boundary ~~on Figs. 1–6~~.

When comparing the data of various experiments in the ERB, the question arises about the compatibility of these results with each other and the reasons for their discrepancies. More or less significant discrepancies in the results of the satellites can be connected with the differences in ~~the~~ their trajectories ~~of the satellites~~; in the construction of the instruments and their angular characteristics; in the energy ranges and sets of ~~the~~ energy channels. For the stationary ERB, these discrepancies can also be associated with differences in the general state of the ~~Solar~~ Sun, heliosphere and magnetosphere of the Earth ~~at the different measurements~~ during various periods of data-taking. These factors influence ~~on~~ the fluxes of ions with $Z \geq 2$ in the ERB more significantly ~~than on the~~ with respect to proton fluxes (see, e.g., Kovtyukh, 2018).

~~This~~ In this section, ~~used~~ experimental data of various satellites, which were obtained for quiet periods (Kp < 2) and near the equatorial plane of the ERB for ions with equatorial pitch angles $\alpha_0 \approx 90^o$ have been used. ~~The preference was given to the averaged results of these satellites for quiet periods. All values of differential fluxes reduced to one dimension.~~ In the regions of E and L shells, where these data were obtained, the ion fluxes ~~do~~ are not distorted by the background of other particles.

In many important experiments, the instruments ~~did not allow~~ were not able to separate fluxes of ions by their charge of ions. ~~For~~ Moreover, for the ions of the CNO group, the separation by mass ~~also~~ are not ~~performing usually~~ usually performed. For heavier ~~ions~~ species, for example for Fe ions, we have very small~~er such~~ data-sets. Therefore, this work presents ~~only~~ data on helium ions (without any charge separating ~~them by charge~~) and ~~ions of~~ CNO ions ~~group~~ (without any mass or charge separation ~~them by mass and charge~~).

To solve the aforementioned problems ~~considered here~~, it is important to choose the form of representation (space of variables), in which the results of ~~different~~ the single experiments can be ~~conformed~~ compared to each other ~~naturally~~. ~~For such representation of the distributions of the ion fluxes have~~ In our case, the space $\{E.\ L\}$ has been used; ~~chosen the space $\{E, L\}$. Such representation is possible~~ this choice is very efficient to better organize ~~of a~~ fragmentary experimental data obtained in different ranges of E and L ~~most effectively~~.

Figures 1–6 presented here the spatial-energy distributions of the fluxes of protons, helium ions, and ions of the CNO group near the equatorial plane. These figures united in pairs: odd figures refer to periods near the minima, and even figures refer to periods near the solar activity maxima. The values E and L in these figures are presented in logarithmic scales. Statistical and methodical errors of the experimentalal points on these figures do not exceed of the size of these points. These points are connected by lines of the equal intensity of ion fluxes (iso-lines); the decimal logarithms of the fluxes J, in unit of (cm^2 s ster MeV/n)$^{-1}$, are shown near each iso-lines. ~~The ion fluxes J have a dimension (cm^2 s ster MeV/n)$^{-1}$ and are corresponded to the energies E (MeV/n) and an equatorial pitch angle of α_0 is ~ 90^o.~~

Such representations of the experimental data are not only visual, but also ~~are~~ very convenient and rather universal. Obviously, Figs. 1–6 actually show both radial profiles of the fluxes of ions for a given energy ~~(if one see along the abscissa axis)~~ and ion energy spectra for a given L shell ~~(if one see along the ordinate axis)~~.

In this place, it is need to say a few words about the method of constructing these figures. The points in Figs. 1–6 ~~are~~ have been obtained from the ~~dependences~~ radial profiles of fluxes $J(L)$ for ~~a given ions with a certain energy (~~the average energies of the ions ~~for each~~ in the channels of the instruments~~) and with an equatorial pitch angle close to 90^o~~. Unlike ~~a distributions of electrons, as well as ion distributions connected with magnetic disturbances~~ electron fluxes or ion fluxes measured during geo-active conditions, ~~the dependences~~ the ion fluxes considered here (i.e. during quiet periods), for ~~the ERB~~ ions ~~with α_0 ~ 90^o~~ usually have only one maximum ~~in a quiet time~~ in the functions $J(L)$. As a result, for each experiment, 1 or 2 points were obtained (on the outer and inner edges of these profiles) with certain values of E and L for a given level of ~~stationary~~ ion fluxes. Sometimes, especially for low ~~levels of~~ fluxes, only one point was obtained: in these cases, the radial profile of the ion fluxes was cutoff at small values of L ~~by~~ due to a significant background of ~~other~~ contaminating particles~~. In these cases,~~ and no interpolation~~s and~~/ extrapolation~~s of the radial profiles of ion fluxes does performing here~~ has been performed whatsoever.

Each iso-line, shown in these figures, ~~was built~~ has been evaluated separately~~, for~~ from the corresponding set of experimental points (icons); after that this iso-line was transferred (along with the icons) to the corresponding figure~~. Thus,~~ ; thus, in ~~the region~~ more abundantly populated sectors of the plots ~~by such icons~~ (i.e. for protons with $E > 1$ MeV at $L > 2$) ~~they~~ such iso-lines are mixing in Figs. 1–2. In ~~the~~ case~~s~~ of a large distance~~s~~ between neighboring points, the corresponding segments of the iso-lines are shown ~~in dotted~~ as dashed arcs ~~in these figures~~.

The radial profiles of the differential fluxes $J(L)$ ~~shown on uniform presentation for~~ of particles ~~of~~ with different ~~energies~~ energy ~~are~~ tend to intersect with each other in those regions where the energy spectra ~~of these fluxes are have a~~ present some local maximum or minimum. ~~In contrast,~~ On the contrary, the ~~flux~~ iso-lines cannot intersect with each other: because this would mean that, at the same point in the space $\{E, L\}$, the ion fluxes differ very significantly (by an order of magnitude ~~for the flux step selected here~~). Such uncertainty does not have a physical sense and ~~means a complete discrepancy and contradiction to each other of two close series of data obtained in different experiments. In this case,~~ a special analysis is needed to identify ~~all the errors and differences in the conditions for different measurements, in order to reconcile them with each other~~ other possible sources of errors.

~~The largest errors of our method are connected with drawing iso-lines of fluxes along heterogeneous sets of experimental points (the errors of these points themselves do not exceed of the size of the icons on Figs. 1–6). This uncertainty of our work is open for constructive criticism, and these figures themselves are open for possible corrections and additions.~~

~~The synthesis of the experimental data on the fluxes of ERB ions in other representations (in other spaces of variables) leads For example, one can present ion fluxes obtained in various experiments for different energy channels depending on L (radial profiles of fluxes). However, the~~

~~sets of these channels are different in different experiments. To compare the radial profiles of ion fluxes for different experiments, it is necessary to bring these fluxes to the same set of energy values. This can made by energy spectra, but due to discreteness of these spectra, the procedures of their approximation, interpolation, and extrapolation are inevitable. But this work can be done in different ways. With that, methodical errors and uncertainties in the final picture acquire a hidden form. They can be tracked only if consistently, step by step, repeating all these procedures for the experimental data.~~

Representing plots in a different space of variables would lead only to more significant methodological errors and uncertainties, because of the natural differences in the instrumentation of the experiments taken into account; thus, a series of approximations or interpolation/extrapolation techniques would become inevitable.

2.1 Spatial-energy structure of the proton fluxes

There is a ~~great quantity~~ large number of ~~the~~ experimental data ~~on the~~ concerning ERB protons~~.~~ ~~The~~ ; the most important of them are presented ~~in the space {E. L} on~~ in Figs. 1 and 2. These figures ~~are needed here for~~ serve as a comparison with similar distributions of ~~ions with~~ $Z \geq 2$ ions (~~on the~~ Figs. 3–6).

Figure 1 represents ~~a~~ results ~~of~~ from the satellites Relay-1 (Freden et al., 1965); Ohzora or EXIS C: Exospheric Satellite C, Akebono or EXOS-D: Exospheric Satellite D and ETS-VI: Engineering Test Satellite (Goka et al., 1999). These results ~~were obtained near minima~~ have been collected during minimum periods of various solar cycles, i.e. between 19th and 20th (1963), 21th and 22th (1984–1985), and 22th and 23th (1994–1996) of the solar activity cycles.

Figure 2 represents ~~a~~ results ~~of~~ from the satellites 1968-81A (Stevens et al., 1970), Injun-5 or Explorer-40 (Krimigis, 1970; Venkatesan and Krimigis, 1971; Pizzella and Randall, 1971), 1969-025C or OV1-19: Orbiting Vehicle 1-19 (Croley et al., 1976), Azur or GRS A: German Research Satellite A (Hovestadt et al., 1972; Westphalen and Spjeldvik, 1982), Molniya-1 (Panasyuk and Sosnovets, 1973), GEOS-2: Geodetic Earth Orbiting Satellite 2 (Wilken et al., 1986), CRRES: The Combined Release and Radiation Effects Satellite (Albert et al., 1998; Vacaresse et al., 1999), GEO-3: Geostationary Orbit 3 (Selesnick et al., 2010) and Van Allen Probes (Selesnick et al., 2014, 2018). These results were obtained ~~near maxima~~ during maximum periods of solar ~~activity in~~ cycles: 20th (1968–1971), 22th (1990–1991), 23th (2000), and 24th (2012–2017) ~~solar cycles~~.

The data of the satellites Explorer-45 (Fritz and Spjeldvik, 1979, 1981) and ISEE-1: International Sun-Earth Explorer 1 or Explorer-56 (Williams, 1981; Williams and Frank, 1984) are given in both Figs. 1 and 2 ~~at $L > 2.5$ where~~ because solar-cyclic variations of the ERB proton fluxes are ~~practically do not observed~~ negligible at $L > 2.5$ (see, e.g., Vacaresse et al., 1999).

~~Other experimental data on the ERB protons could be added to these results, but they do not change the general picture shown in Figs. 1 and 2.~~

From a comparison of Figs. 1 and 2 one can see that at $L < 2.5$ (especially at $L < 1.4$) the proton fluxes ~~in the minima of~~ during solar ~~activity~~ minima (Fig. 1) are higher than ~~in the~~ during maxima ~~of solar activity~~ (Fig. 2). In addition, in the ~~minima of solar activity~~ former the inner edge of the proton belt is less steep and ~~achieve~~ it can reach smaller L shells (for $E > 1$ MeV). The distributions ~~functions~~ of protons ~~$f(\mu, K, L)$~~ in the ~~phase~~ space $\{\mu, L\}$ (see, e.g., Kovtyukh,(2016a,b) which I constructed from Figs. 1 and 2 confirm these conclusions.

In Figs. 1 and 2, the iso-lines of proton fluxes are almost parallel to each other on $L > 3$ at sufficiently high energies. Since these iso-lines have separated from each other by approximately equal intervals on a logarithmic scale of the energy, this region in the space $\{E. L\}$ corresponds to power-law spectra of the ERB protons: for power-law spectra, $J \propto E^{-\gamma}$, index $\gamma = -\Delta(\log J)/\Delta(\log E)$. In these figures, this region is located between the green and red lines.

The red line ~~is corresponded~~ corresponds to the lower boundary (E_b) of the power-law tail of the proton spectra. For this line, $E_b \sim 36\times L^{-3}$ MeV. Some changes in the slope of these iso-lines at $L >$

6 can be connected ~~with an essential distinction of the~~ to a discrepancy between the real configuration of the magnetic field lines of the magnetic field ~~in this region from the dipole~~ and the dipolar configuration (~~the~~ used here for L shells calculation ~~were calculated for a dipole field~~).

For the dipole magnetic field region, the points on the red line correspond to particles with a specific value of the 1st adiabatic invariant of motion (μ_b). For Figs. 1 and 2, the average value μ_b is ~ 1.16 keV nT^{-1}. Segments of an iso-lines that are parallel to the red line also correspond to ~~a~~ certain values of the invariant μ. In this region of the space $\{E. L\}$ the ionization and other losses of the ERB protons during radial drift can be neglected, and ~~the fluxes~~ changes of fluxes with changing ~~of~~ L are practically reduced to adiabatic transformations ~~the fluxes~~ in a magnetic field.

It ~~is~~ results from these figures that at L = 3–6 the value $\gamma = 4.8 \pm 0.5$. At $L > 6$ the distances between these iso-lines are increase~~d~~ with L, and the value γ is decreased from ~ 4.7–5.0 at L = 6 to ~ 4.1–4.5 at L = 8. This is due to the deviation of the magnetic field from the dipole configuration as well as to the increasing variability of this field with increasing L.

According to the data of satellites considered in (Kovtyukh, 2001), invariant parameters μ_b and γ were found only at $L > 3$. In this work, ~~is considered the~~ a wider range of L and E is considered, and for protons with $E > 10$ MeV these parameters can be traced to $L \sim 2$. At $L = 2$, $\gamma = 4.4 \pm 0.6$ (Fig. 1) and $\gamma = 4.7 \pm 1.3$ (Fig. 2). This is due to the fact that the energy range ~~here~~ is significantly extended toward higher ~~energies~~ values (up to 200 MeV), but ~~with increasing the energy of the ERB protons here~~ the ionization losses ~~are decreased rapidly~~ for protons rapidly decrease (see, e.g., Schulz and Lanzerotti, 1974; Kovtyukh, 2016a).

2.2 Spatial-energy structure of the helium ion fluxes

In Figs. 3 and 4 ~~are presented~~ helium ions fluxes averaged for quiet periods (Kp < 2) are presented.

Figure 3 represents ~~the data of~~ results from the satellites Molnija-2 (Panasyuk et al., 1977), Prognoz-5 (Lutsenko and Nikolaeva, 1978), ISEE-1: The International Sun-Earth Explorer 1 (Hovestadt et al., 1981); Akebono or EXOS-D: Exospheric Satellite D and ETS-VI: Engineering Test Satellite (Goka et al., 1999). These results ~~were obtained near minima~~ have been collected during minimum periods of various solar cycles, i.e. between 20th and 21th (1975–1977), between 21th and 22th (1984–1985), and between 22th and 23th (1994–1996) of the solar activity cycles.

Figure 4 represents ~~the data of~~ results from the satellites OV1-19: Orbiting Vehicle 1-19 (Blake et al., 1973; Fennell and Blake, 1976), Explorer-45 (Fritz and Spjeldvik, 1978, 1979; Spjeldvik and Fritz, 1981), SCATHA: Spacecraft Charging At High Altitudes (Blake and Fennell, 1981; Chenette et al., 1984). These results were obtained ~~near maxima~~ during maximum periods of solar ~~activity in~~ cycles: 20th (1968–1971) and 21th (1979) ~~solar cycles~~.

From a comparison of Figs. 1–2 with Figs. 3–4 one can see that at $L > 2$ for helium ions the solar-cyclic (11-year) variations are greater than for protons. For example, at $L \sim 2$–3 from maximum to minimum of solar activity fluxes of protons with $E > 1$ MeV practically do not changed, and the fluxes of helium ions with $E > 1$ MeV/n are increased by one order of magnitude.

Figures 3 and 4 have the same patterns ~~are observed~~ as for protons, but the distribution of helium ion fluxes is slightly shifted ~~away from the Earth~~ towards higher values of L shell (with respect to protons). Unlike protons, there are significant "white spots" in these figures: ~~for helium ions in this picture~~ no experimental data for helium ions in these regions.

The red line on these figures ~~is~~ correspond~~ed~~s to the lower boundary of the power-law tail of the helium ions spectra. For this line, $E_b/M_i \sim 43.4 \times L^{-3}$ MeV/n (Fig. 3) and $E_b/M_i \sim 21.7 \times L^{-3}$ MeV/n (Fig. 4). If one takes into account that at $L < 6$ for helium ions with $E > 0.2$ MeV/n the average charge $Q_i = +2$ (see, e.g, Spjeldvik, 1979), then for the considered boundary we get: $\mu_b \sim 1.4 \times Q_i$ keV/n×nT^{-1} at the maximum of solar activity and $\mu_b \sim 1.4 \times M_i$ keV/n×nT^{-1} at the minimum of solar activity (for the dipole magnetic field region). The iso-lines of helium ion fluxes in Figs. 3 and 4, which pass above the red line at $L > 2.5$, ~~are~~ correspond~~ed~~ to an average value of $\gamma \sim 5.5$.

For helium ions spectra, as for protons ones, the values of the parameters of the power-law tail ~~of their spectra are approximately in the middle of the ranges of these parameters, which were obtained by other methods~~ are in good agreement with what has been found in (Kovtyukh, 2001).

At the same time, one can see that the iso-lines of the fluxes of helium ions in the region above the red line (in the region of power-law spectra) ~~have at a~~ substantial deviate from the slope ~~to~~ of the red line. At $L > 3$ the fluxes of helium ions with given energy are increase~~d~~ with decreasing L ~~more slowly~~ slower than ~~follows~~ expected from adiabatic transformation~~s of the fluxes~~ (see Kovtyukh, 2001). This means that the ionization losses of the ERB helium ions significantly exceed these losses for protons, in agreement ~~In accordance~~ to well-known calculations (see, e.g., Schulz and Lanzerotti, 1974)~~, this is means that the ionization losses of the ERB helium ions significantly exceed these losses for protons~~.

2.3 Spatial-energy structure of the CNO group ions fluxes

In Figs. 5 and 6 ~~are presented~~ CNO group ions fluxes averaged for quiet periods (Kp < 2) are presented.

Figure 5 represents ~~the data of~~ results from the satellites ATS-6: Applications Technology Satellite 6 (Spjeldvik and Fritz, 1978; Fritz and Spjeldvik, 1981) and ISEE-1: The International Sun-Earth Explorer 1 (Hovestadt et al., 1978). These results ~~were obtained near the minimum~~ have been collected during minimum period between 20th and 21th of the solar activity cycles (1974–1975, 1977).

Figure 6 represents ~~the data of~~ results from the satellite Explorer-45 (Spjeldvik and Fritz, 1978; Fritz and Spjeldvik, 1981). These results were obtained ~~near the~~ during maximum period of solar activity in 20th solar cycle (1971–1972).

On Figs. 5–6 the spatial-energy patterns of the ion fluxes ~~for~~ of the CNO group ~~ions~~ are even more shifted ~~away from the Earth~~ towards higher values of L shell and its configuration differ significantly from ~~the~~ Figs. 1–4.

From a comparison of Figs. 1–2 with Figs. 5–6 one can see that for ions of CNO group the solar-cyclic (11-year) variations are greater than for protons. For example, at $L \sim 3$–5 from maximum to minimum of solar activity fluxes of protons with $E > 1$ MeV practically do not changed, but the fluxes of the CNO group ~~ions are~~ increase by one order of magnitude ~~and~~ or more. From a comparison of Figs. 3–4 with Figs. 5–6 it is seen also that the fluxes of CNO group ~~ions varies by~~ change several times ~~greater~~ more than the fluxes of helium ions do.

This ~~is~~ means that for ions of the CNO group the ionization losses at $L = 3$–5 are much larger than for ions with $Z \leq 2$ and these losses have a significant effect even on the power-law segment of the spectra of the CNO ions (in the part which is seen on Figs. 5–6). Therefore, the lower boundary of the power-law tail of these ions spectra have not monitored on the data given in Figs. 5 and 6. The red line on these figures ~~is rather arbitrary: it~~ corresponds to adiabatic laws (see Kovtyukh, 2001); ~~that are not performed here, but~~ this line let us ~~to trace~~ estimate the deviations from these laws. As can be seen from Fig. 5–6, ionization losses for ions of the CNO group are especially large at the maximum of solar activity (Fig. 6): in these times the slope of iso-lines on $L > 3$ is significantly less than the slope of the red line.

At the same time, at $L > 4$ in Fig. 5 and at $L > 3$ in Fig. 6 the iso-lines of fluxes pass almost parallel to each other and at approximately equal distances from each other; the average value of γ corresponding to them is ~ 6. Thus, for sufficiently large values of E and L, the CNO group ions spectra in the ERB have a power-law form, but these spectra are softer in comparison with the spectra of protons.

The red line corresponds here to the dependences $E_b/M_i \approx 43.4 \times L^{-3}$ MeV/n (on Fig. 5) and $E_b/M_i \sim 12.4 \times L^{-3}$ MeV/n (on Fig. 6), which are taken from (Kovtyukh, 2001) where this boundary was more clearly defined also for the ions of the CNO group. If one takes into account that at $L \sim 3$–5 for the CNO group ions with $E > 0.1$ MeV/n the average charge $Q_i = +4$ (see, e.g., Spjeldvik and

Fritz, 1978), then for this boundary one can get: $\mu_b \sim 1.4\times Q_i$ keV/n×nT^{-1} at the maximum of solar activity and $\mu_b \sim 1.4\times M_i$ keV/n×nT^{-1} at the minima of solar activity (for the dipole magnetic field region).

3 Discussion

Let us consider the conclusions following from the results obtained here for solar-cyclic variations in the fluxes of ERB ions. Solar-cyclic (11-year) variations of proton fluxes with $E > 1$ MeV in the inner region of the ERB ~~considered~~ have been studied in many works (see, e.g., Pizzella et al., 1962; Hess, 1962; Blanchard and Hess, 1964; Filz, 1967; Nakano and Heckman, 1968; Vernov, 1969; Dragt, 1971; Huston et al., 1996; Vacaresse et al., 1999; Kuznetsov et al., 2010; Qin et al., 2014). These variations ~~achieve~~ reach one order of magnitude at $L = 1.14$ and reduce rapidly with increasing L (see, e.g., Vacaresse et al., 1999).

In these works, such variations of the proton fluxes of the inner belt are connected to the solar-cyclic variations of the energy loss rates of protons in this region. However, solar-cyclic variations of fluxes of ions with $Z \geq 2$ have not considered in these works.

In quiet periods, only the mechanism of ionization losses is significant for the ERB protons trapped on small L shells (see, e.g., Schulz and Lanzerotti, 1974). Energy loss rates and lifetimes of the ERB protons are determined in this mechanism by the density of atmospheric atoms and ionospheric plasma (N) in a geomagnetic trap. This density ~~is~~ depends on the intensity of the ultraviolet radiation of the Sun.

With decreasing solar activity (with a transition from maximum to minimum of the solar cycle), the densities of atmospheric atoms and ionospheric plasma in a geomagnetic trap are decrease~~d~~. If the proton supply rates to the inner belt under the action of the CRAND mechanism remain unchanged or the effect of these changes is weaker than the effect connected with changes of loss rates of the protons, the stationary proton fluxes will increase~~d~~ with decreasing the solar activity ~~decreasing~~.

The lifetimes of protons increase with L, and ~~it lead~~ this leads to ~~decreasing~~ a decrease in the amplitude of the solar-cyclic variations of ~~a~~ proton fluxes. The proton lifetime on a given L shell depends on ~~their~~ its energy and is less than 11 years at $L < L^*(E)$. For example, for protons with $E \sim 10$ MeV the value L^* is ~ 2.5 (see, e.g., Kovtyukh, 2016a). Figs. 1 and 2 show that for protons the solar-cyclic variations of fluxes are small and localized at $L < 2.5$ (mainly at $L < 1.4$).

In contrast to protons, Figs. 3–6 show significant solar-cyclic variations of fluxes of helium ions and CNO group ions at $L \sim 2$–5. These variations ~~one~~ can be explained by the same mechanism~~,~~ ~~which~~ that has been suggested for protons ~~fluxes~~ at $L < 2.5$.

For ions with $Z \geq 2$ in the ERB, ionization losses are more significant than for protons~~. The~~ and this can be connected to the absence of ions with $Z \geq 2$ at $L < 2$ (or very low values of these fluxes) during quiet geomagnetic conditions ~~one can connect with this fact~~. ~~More~~ Such short lifetimes ~~of these ions compare to protons~~ are manifested also in the slope of the experimental curves in Fig. 4 and 6 (this was note in sections 2.2 and 2.3, respectively). Consequently, for ions with $Z \geq 2$, the regions in which ~~the solar-cyclic~~ variations can manifest~~ed~~, should be located on higher L shells (at the same energies as for protons).

The lifetimes of ions ~~of~~ in the ~~energies~~ energy ranges considered here are $\tau \propto M_i^{-1/2} Q_i^{-2} N^{-1} E^{3/2}$ (Schulz and Lanzerotti, 1974). In a first approximation, for $N \propto L^{-4}$, we obtain the value $L_i^* \sim (M_i^{1/2} Q_i^2)^{1/4} L^*$, where L^* corresponds to protons of the same energy ~~as other ions~~ of the other ions under study. For helium ions ($M_i = 4$, $Q_i = 2$) with $E \sim 10$ MeV, we obtain $L_i^* \sim 4.2$. For ions of CNO group ($M_i = 14$, $Q_i = 4$) with $E \sim 10$ MeV we obtain $L_i^* \sim 6.9$. These ~~is~~ are very rough ~~estimates~~ estimations, but they ~~correspond to~~ are in agreement with the results presented in Figs. 3–6.

These estimates are based on the following assumption: during variations in solar activity, the rates of ion supply on $L < L_i^*$ remain unchanged (or these changes are weaker than the effect of changes of the rate of ion losses). This assumption is real for protons with E > 10–20 MeV at L < 2.2~~:~~ ; in fact, the fluxes of these protons form~~ing~~ mainly under the action of the CRAND mechanism. However, at L > 2.2 the stationary ion fluxes of the ERB form~~ing~~ mainly under the action of radial diffusion (see, e.g., Schulz and Lanzerotti, 1974; Kovtyukh, 2016b, 2018). Therefore, the solar-cyclic variations of ~~fluxes for ions with~~ $Z \geq 2$ ion fluxes ~~one~~ can be ~~explain~~ motivated only under the assumption that the effect ~~connected~~ related with an ~~increasing~~ increase in the ionization losses of such ions significantly exceeds the effect connected with the possible enhance of radial diffusion of ions on the ~~growth~~ rising phase of solar activity.

In the experimental results presented here for the ERB ions, the region of the power-law tail of the ion spectra is distinguished. For many experiments, especially for heavy ions, the values of the parameter of a power-law tail spectra are determined much more accurately by the dependences $J(L)$ of the ion fluxes (in ~~the~~ logarithmic scale) for different pairs of energy channels (see Kovtyukh, 2001). For example, the range of L, in which these dependences for two energy channels are parallel to each other is ~~corresponded~~ connected to the power-law tail of the spectra. ~~On~~ Instead, on smaller values of L these fluxes begin to converge and the radial dependences of ~~the~~ these fluxes intersect with each other, which is ~~corresponded~~ related to the maximum in the spectra. ~~Consider here the physical mechanisms leading to the formation of power-law distributions of ions of the ERB.~~

The main source of ions in the outer regions of the ERB is the solar wind, and usually the high-energy part of these spectra have an exponential shape ~~usually~~ (see, e.g., Ipavich et al., 1981a, 1981b). Immediately before being captured into the magnetosphere, these ions pass through a highly turbulized regions, but the high-energy part of their spectra usually retains an exponential shape. Therefore, the question arises: what physical mechanism converts the form of ion spectra from exponential to power-law?

Evidently, the power-law tail of the ERB ions spectra must be generate in the outer regions of the magnetosphere. The most likely region for this to happen is the plasma sheet (PS) of the magnetospheric tail, which is adjacent to the geomagnetic trap. High-energy part of the ion spectra in the PS, at $R \sim 20$–40 R_E, have power-law shape and the exponents of these spectra ~~is~~ are close to the corresponding parameters of the spectra of ions in the ERB. On the data of the satellites IMP-7 and IMP-8~~: Interplanetary Monitoring Platform 7 and 8~~ (Sarris et al., 1981; Lui et al., 1981) and also satellite ISEE-1 (Christon et al., 1991), the shape of the ion spectra of the PS usually do not change~~d~~ during substorms; they produce only parallel shifts of the spectra along logarithmic axes E and J. These results point out that the time scales of formation processes of these ion spectra in the PS ~~are far~~ exceed~~s~~ the times of substorms.

Parameters of the power-law tail of the ion spectra of the outer belt (γ and μ_b) reflect, apparently, the most fundamental features of the mechanisms of acceleration of ions in the tail of the magnetosphere. One can try to connect the values of these parameters with the most general representations ~~about~~ of the mechanisms ~~and character~~ of ion acceleration in the PS of the magnetospheric tail.

Most likely, this part of the ion energy spectra is formed in the PS by stochastic mechanisms of ~~the~~ ion acceleration~~. This~~ ; this hypothesis is supported by many experimental results. ~~Statistical character~~ The statistical aspect of these mechanisms reveals itself, in particular, in the fact that the ratios of fluxes (and partial densities) of ions with different Z can ~~be~~ differ, even greatly, at low and high energies. During their wander in the phase space, ions gradually ~~forget~~ loose information about their origin and, therefore, the high-energy tails of ~~the ion~~ their spectra ~~do not~~ contain ~~un~~ambiguous information on the partial densities of different components of ions in the source (see, e.g., Kovtyukh, 2001).

The high-energy ~~part~~ portion of the ion spectra of the PS can be generated by the mechanisms of acceleration of particles on magnetic irregularities moving ~~relative~~ with respect to each other

(Fermi mechanism). The fractal structures of the PS are revealed ~~itself~~ on scales from ~ 0.4 to ~ 8 thousands kilometers, for example, in the data of the satellite Geotail (Milovanov et al., 1996). If the mass of the ions are small compared to the masses of the magnetic irregularities in the PS, the average values of the index γ of the power-law tail ~~of the spectra~~ should not depend on mass and charge of ~~these ions~~ such nuclei.

Under equilibrium conditions, this parameter is determined by the average part of energetic ions in the total energy density of particles and magnetic irregularities ($\overline{\beta}$). From the theory which was developed by Ginzburg and Syrovatskii (1964), it ~~is~~ follows: $\gamma - 1 \approx (1 - \overline{\beta})^{-1}$. With increasing $\overline{\beta}$ in the interval $0 < \overline{\beta} < 1$, the value γ ~~is~~ increases monotonically and $\gamma \to \infty$ for $\overline{\beta} \to 1$. For real average values $\overline{\beta}$ in the central PS, we get $\gamma \sim 3.5$–7.0 ($\gamma \sim 4.3$ at $\overline{\beta} \sim 0.7$).

Spectra with power-law tail and quasi-exponential segment at lower energies can be generated when the value $\Delta B / \overline{B}$ for magnetic irregularities is proportional to their size δr and ~~the~~ their spectral density ~~of irregularities is~~ decrease rapidly with increasing δr for $\delta r < r_s$, but for $\delta r > r_s$ it remains almost unchanged. Apparently, the spectra of magnetic irregularities in PS with thickness r_s have just such form. Then the lower boundary μ_b of the power-law tail ~~is corresponded~~ corresponds to the condition $r_s/\rho_i \sim 10$ (ρ_i is the gyroradius of ions), i.e. $\mu_b \sim 0.02(Q_i^2/M_i)B_s r_s^2$ keV nT^{-1}, where B_s is the average magnetic field induction in the PS (in nT) and r_s is normalized to the Earth's radius. Believing that $B_s \sim 30$ nT and $r_s \sim 1.3$ R_E it can be obtained: $\mu_b \sim 1.0$ (Q_i^2/M_i) keV nT^{-1}.

The energy spectra of ions in the radiation belts of such planets as Jupiter and Saturn have the form analogous to ~~the form~~ that of ion spectra in the ERB (see, e.g., Krimigis et al., 1981; Cheng et al., 1985). As that in the ERB, these spectra have a long power-law tail, which is formed, apparently, by mechanisms of stochastic acceleration of ions as a result of interactions of these ions with the current layer of the magnetospheric tail.

5 Conclusions

~~There are analyzed~~ In this work, the experimental results for the stationary fluxes of the main ion components of the ERB (protons, helium ions and ions of the CNO group) in the near equatorially plane, have been analyzed. It is found that in the outer belt these fluxes line up in the certain regular patterns in the space $\{E, L\}$. The degree of such similarity ~~is~~ increases with increasing E and L~~. The similarity of the spatial-energy distributions for various ionic components of the ERB is based on~~ and it is linked to the nature of the main sources and on the universality mechanisms of transfer, acceleration and losses of ERB ions in the outer belt (radial diffusion while conserving μ and K of ions, betatron acceleration and ionization losses).

~~Solar-cyclic~~ Moreover, solar-cyclic (11-year) variations of the spatial-energy distributions of the ERB ion fluxes ~~are~~ have been investigated. It ~~is find~~ has been noted that the ERB ions fluxes are ~~weaken~~ weaker with increasing ~~the~~ solar activity and this effect increases with increasing ~~an~~ atomic number Z ~~of the ions~~. Such a dependence of the amplitude of flux changes on Z is typical, also, for faster variations in the fluxes of the ERB ions, during geomagnetic storms and other disturbances of the Earth's magnetosphere, ~~what is~~ as has been underlined in the review Kovtyukh (2018).

The figures presented here make it possible to determine in which regions of the space $\{E, L\}$ near the equatorial plane the ionization losses of ions during their radial diffusion can be neglected and where this cannot. These results indicate also that with variations in the level of solar activity the coefficient D_{LL} of the radial diffusion of the ERB ions change much less than the ionization losses rates of ions with $Z \geq 2$.

In addition, the figures given here reveal the localization of "white spots", especially extensive for ions with $Z \geq 2$ and $E > 1$ MeV/n at $L < 3$. ~~The larger~~ As Z and energy ~~of ions~~ become larger and ~~the~~

~~smaller~~ L becomes smaller, ~~the greater~~ the ~~uncertainty~~ uncertainties in the values of the ERB fluxes become larger. These gaps must be filled by the results of ~~the~~ future experiments on ~~the~~ satellites~~.~~ ~~Now~~ ; for now, the extensive gaps in the experimental data for fluxes of ions with $Z \geq 2$ do not allow to create ~~the~~ sufficiently complete and reliable empirical models of the ERB for these ions.

Acknowledgements.

Financial support. This work was supported by Russian Foundation for Basic Research RFFI grant No. 17-29-01022.

References

Alfvén, H., and Fälthammar, C.-G.: Cosmical Electrodynamics, Fundamental Principles, Clarendon Press, Oxford, 1963.

Albert, J. M., Ginet, G. P., and Gussenhoven, M. S.: CRRES observations of radiation belt protons, 1, Data overview and steady state radial diffusion, J. Geophys. Res., **103**(A5), 9261–9273. https://doi.org/10.1029/97JA02869, 1998.

Blake, J. B., and Fennell, J. F.: Heavy ion measurements in the synchronous altitude region, Planet. Space Sci., **29**(11), 1205–1213, https://doi.org/10.1016/0032.0633(81)90125-2, 1981.

Blake, J. B., Fennell, J. F., Schulz, M., and Paulikas, G. A.: Geomagnetically trapped alpha particles, 2, The inner zone, J. Geophys. Res., **78**(25), 5498–5506, https://doi.org/10.1029/JA078i025p05498, 1973.

Blanchard, R. C., and Hess, W. N.: Solar cycle changes in inner-zone protons, J. Geophys. Res., **69**(19), 3927–3938, https://doi.org/10.1029/JZ069i019p03927, 1964.

Chenette, D. L., Blake, J. B., and Fennell, J. F.: The charge state composition of 0.4–MeV helium ions in the Earth's outer radiation belts during quiet times, J. Geophys. Res., **89**(A9), 7551–7555, https://doi.org/10.1029/JA089iA09p07551, 1984.

Cheng, A. F., Krimigis, S. M., and Armstrong, T. P.: Near equality of ion phase space densities at Earth, Jupiter, and Saturn, J. Geophys. Res., **90**(A9), 526–530, http://doi.org/10.1029/JA090iA01p00526, 1985.

Christon, S. P., Williams, D. J., Mitchell, D. G., Huang, C. Y., and Frank, L. A.: Spectral characteristics of plasma sheet ion and electron populations during disturbed geomagnetic conditions, J. Geophys. Res., **96**(A1), 1–22, https://doi.org/10.1029/90JA01633, 1991.

Croley, D. R., Jr., Schulz, M., and Blake, J. B.: Radial diffusion of inner-zone protons: Observations and variational analysis, J. Geophys. Res., **81**(4), 585–594, https://doi.org/10.1029/JA081i004p00585, 1976.

Dragt, A. J.: Solar cycle modulation of the radiation belt proton flux, J. Geophys. Res., **76**(10), 2313–2344, https://doi.org/10.1029/JA076i010p02313, 1971.

Fennell, J. F., and Blake, J. B.: Geomagnetically trapped α-particles, Magnetospheric Particles and Fields, edited by: McCormac, B. M., D. Reidel, Dordrecht, Holland, 149–156, 1976.

Filz, R. C.: Comparison of the low-altitude inner-zone 55–MeV trapped proton fluxes measured in 1965 and 1961–1962, J. Geophys. Res., **72**(3), 959–963, https://doi.org/10.1029/JZ072i003p00959, 1967.

Freden, S. C., Blake, J. B., and Paulikas, G. A.: Spatial variation of the inner zone trapped proton spectrum, J. Geophys. Res., **70**(13), 3113–3116, https://doi.org/10.1029/JZ070i013p03113, 1965.

Fritz, T. A., and Spjeldvik, W. N.: Observations of energetic radiation belt helium ions at the geomagnetic equator during quiet conditions, J. Geophys. Res., **83**(A6), 2579–2583, https://doi.org/10.1029/JA083iA06p02579, 1978.

Fritz, T. A., and Spjeldvik, W. N.: Simultaneous quiet time observations of energetic radiation belt protons and helium ions: The equatorial α/p ratio near 1 MeV, J. Geophys. Res., **84**(A6), 2608−2618, https://doi.org/10.1029/JA084iA06p02608, 1979.

Fritz, T. A., and Spjeldvik, W. N.: Steady-state observations of geomagnetically trapped energetic heavy ions and their implications for theory, Planet. Space Sci., **29**(11), 1169–1193, https://doi.org/10.1016/0032-0633(81)90123-9, 1981.

Ginzburg, V. L., and Syrovatskii, S. I.: The Origin of Cosmic Rays, Pergamon Press, Oxford, 1964.

Ginet, G. P., O'Brien, T. P., Huston, S. L., Johnston, W. R., Guild, T. B., Friedel, R., Lindstrom, C. D., Roth, C. J., Whelan, P., Quinn, R. A., Madden, D., Morley, S., and Su, Yi-J.: AE9, AP9 and SPM: New models for specifying the trapped energetic particle and space plasma environment, Space Sci. Rev., **179**(1–4), 579–615, https://doi.org/10.1007/s11214-013-9964-y, 2013.

Goka, T., Matsumoto, H., and Takagi, S.: Empirical model based on the measurements of the Japanese spacecrafts, Radiation Measurements, **30**(5), 617–624, https://doi.org/10.1016/S1350-4487(99)00237-1, 1999.

Hess, W. N.: Discussion of paper by Pizzella, McIlwain, and Van Allen, 'Time variations of intensity in the Earth's inner radiation zone, October 1959 through December 1960', J. Geophys. Res., **67**(12), 4886–4887, https://doi.org/10.1029/JZ0670i012p04886, 1962.

Hovestadt, D., Häusler, B., and Scholer, M.: Observation of energetic particles at very low altitudes near the geomagnetic equator, Phys. Rev. Lett., **28**(20), 1340–1343, https://doi.org/10.1103/PhysRevLett.28.1340, 1972.

Hovestadt, D., Gloeckler, G., Fan, C. Y., Fisk, L. A., Ipavich, F.M., Klecker, B., O'Gallagher, J. J., and Scholer, M.: Evidence for solar wind origin of energetic heavy ions in the Earth's radiation belt, Geophys. Res. Lett., **5**(12), 1055–1057, https://doi.org/10.1029/GL005i012p01055, 1978.

Hovestadt, D., Klecker, B., Mitchell, E., Fennell, J. F., Gloeckler, G., and Fan, C. Y.: Spatial distribution of $Z \geq 2$ ions in the outer radiation belt during quiet conditions, Adv. Space Res., **1**(1), 305–308, https://doi.org/10.1016/0273-1177(81)90125-3, 1981.

Huston, S., Kuck, G., and Pfitzer, K.: Low-altitude trapped radiation model using TIROS/NOAA data, Radiation Belts: Models and Standards, edited by: Lemaire, J. F., Heynderickx, D., and Baker, D. N., AGU, Washington, D. C., 119–122, https://doi.org/10.1029/GM097/p0119, 1996.

Ilyin, B. D., Kuznetsov, S. N., Panasyuk, M. I., and Sosnovets, E.N.: Non-adiabatic effects and boundary of the trapped protons in the Earth's radiation belts, Bulletin of the Russian Academy of Sciences: Physics, **48**(11), 2200–2203, 1984.

Ipavich, F. M., Galvin, A. B., Gloeckler, G., Scholer, M., and Hovestadt D.: A statistical survey of ions observed upstream of the Earth's bow shock: Energy spectra, composition, and spatial variation, J. Geophys. Res., **86**(A6), 4337–4342, https://doi.org/10.1029/JA086iA06p4337, 1981a.

Ipavich, F. M., Scholer, M., and Gloeckler, G.: Temporal development of composition, spectra, and anisotropies during upstream particle events, J. Geophys. Res., **86**(A13), 11153–11160, https://doi.org/10.1029/JA086iA13p11153, 1981b.

Kovtyukh, A. S.: Geocorona of hot plasma, Cosmic Res., **39**(6), 527−558, https://doi:10.1023/A:1013074126604, 2001.

Kovtyukh, A. S.: Radial dependence of ionization losses of protons of the Earth's radiation belts, Ann. Geophys., **34**(1), 17–28, https://doi.org/10.5194/angeo-34-17-2016, 2016a.

Kovtyukh, A. S.: Deduction of the rates of radial diffusion of protons from the structure of the Earth's radiation belts, Ann. Geophys., 34(11), 1085–1098. https://doi:10.5194/angeo-34-1085-2016, 2016b.

Kovtyukh, A. S.: Ion Composition of the Earth's Radiation Belts in the Range from 100 keV to 100 MeV/nucleon: Fifty Years of Research, Space Sci. Rev., **214**(8), 124:1–124:30, https:/doi.org/10.1007/s11214-018-0560-z, 2018.

Krimigis, S. M.: Alpha particles trapped in the Earth's magnetic field, Particles and Fields in the Magnetosphere, edited by: McCormac, B. M., D. Reidel, Dordrecht, Holland, 364−379, 1970.

Krimigis, S. M., Carbary, J. F., Keath, E. P., Bostrom, C. O., Axford, W. I., Gloeckler, G., Lanzerotti, L. J., and Armstrong, T. P.: Characteristics of hot plasma in the Jovian magnetosphere: Results from the Voyager spacecraft, J. Geophys. Res., **86**(A10), 8227−8257. http://doi.org/10.1029/JA086iA10p08227, 1981.

Kuznetsov, N. V., Nikolaeva, N. I., and Panasyuk, M. I.: Variation of the trapped proton flux in the inner radiation belt of the Earth as a function of solar activity, Cosmic Res., **48**(1), 80–85, https://doi.org/10.1134/S0010952510010065, 2010.

Lui, A. T. Y., and Krimigis, S. M.: Several features of the earthward and tailward streaming of energetic protons (0.29−0.5 MeV) in the Earth's plasma sheet, J. Geophys. Res., **86**(A13), 11173−11188, https://doi.org/10.1029/JA086iA13p11173, 1981.

Lutsenko, V. N., and Nikolaeva, N. S.: Relative content and the range of alpha particles in the inner radiation belt of the Earth by measurements on satellite Prognoz-5, Cosmic Res., **16**(3), 459–462, 1978.

McIlwain, C. E.: Coordinate for mapping the distribution of magnetically trapped particles, J. Geophys. Res., **66**(11), 3681–3691, https://doi.org/10.1029/JZ066i011p03681, 1961.

Milovanov, A. V., Zelenyi, L. M., and Zimbardo, G.: Fractal structures and power low spectra in the distant Earth's magnetotail, J. Geophys. Res. Space Phys., **101**(A9), 19903−19910, https://doi.org/10.1029/96JA01562, 1996.

Nakano, G., and Heckman, H.: Evidence for solar-cycle changes in the inner-belt protons, Phys. Rev. Lett., **20**(15), 806–809, https://doi.org/10.1103/PhysRevLett.20.806, 1968.

Northrop, T. G.: The Adiabatic Motion of Charged Particles, Wiley-Interscience, NY, USA, 1963.

Panasyuk, M. I., and Sosnovets, E. N.: Differential energy spectrum of low-energy protons in the inner region of the radiation belt, Cosmic Res., **11**(3), 436−440, 1973.

Panasyuk, M. I., Reizman, S. Ya., Sosnovets, E. N., and Filatov, V. N.: Experimental results of protons and α-particles measurements with energy more 1 MeV/nucleon in the radiation belts, Cosmic Res., **15**(6), 887–894, 1977.

Pizzella, G., McIlwain, C. E., and Van Allen, J. A.: Time variations of intensity in the Earth's inner radiation zone, October 1959 through December 1960, J. Geophys. Res., **67**(4), 1235–1253, https://doi.org/10.1029/JZ0670i004p01235, 1962.

Pizzella, G., and Randall, B. A.: Differential energy spectrum of geomagnetically trapped protons with the Injun 5 satellite, J. Geophys. Res., **76**(10), 2306−2312, https://doi.org/10.1029/JA076i010p02306, 1971.

Qin, M., Zhang, X., Ni, B., Song, H., Zou, H., and Sun, Y.: Solar cycle variations of trapped proton flux in the inner radiation belt, J. Geophys. Res. Space Phys., **119**(12), 9658–9669, https://doi.org/10.1002/2014JA020300, 2014.

Sarris, E. T., Krimigis, S. M., Lui, A. T. Y., Ackerson, K. L., Frank, L. A., and Williams, D. J.: Relationship between energetic particles and plasmas in the distant plasma sheet, Geophys. Res. Lett., **8**(4), 349–352, https://doi.org/10.1029/GL008i004p0349, 1981.

Schulz, M., and Lanzerotti, L. J.: Particle Diffusion in the Radiation Belts, Springer, NY, USA, 1974.

Selesnick, R. S., Hudson, M. K., and Kress, B. T.: Injection and loss of inner radiation belt protons during solar proton events and magnetic storms, J. Geophys. Res. Space Phys., **115**(A8), A08211, https://doi.org/10.1029/2010JA015247, 2010.

Selesnick, R. S., Baker, D. N., Jaynes, A. N., Li, X., Kanekal, S. G., Hudson, M. K., and Kress, B. T.: Observations of the inner radiation belt: CRAND and trapped solar protons, J. Geophys. Res. Space Phys., **119**(8), 6541–6552, https://doi.org/10.1002/2014JA020188, 2014.

Selesnick, R. S., Baker, D. N., Kanekal, S. G., Hoxie, V. C., and Li, X.: Modeling the proton radiation belt with Van Allen Probes Relativistic Electron-Proton Telescope data, J. Geophys. Res. Space Phys., **123**(1), 685–697, https://doi.org/10.1002/2017JA024661, 2018.

Spjeldvik, W. N.: Expected charge states of energetic ions in the magnetosphere, Space Sci. Rev., **23**(3), 499−538, https://doi.org/10.1007/BF00172252, 1979.
Spjeldvik, W. N., and Fritz, T. A.: Quiet time observations of equatorially trapped megaelectronvolt radiation belt ions with nuclear charge $Z \geq 4$, J. Geophys. Res., **83**(A9), 4401–4405, https://doi.org/10.1029/JA083iA09p04401, 1978.
Spjeldvik, W. N., and Fritz, T. A.: Observations of energetic helium ions in the Earth's radiation belts during a sequence of geomagnetic storms, J. Geophys. Res., **86**(A4), 2317−2328, https://doi.org/10.1029/JA086iA04p02317, 1981.
Stevens, J. R., Martina, E. F., and White, R. S.: Proton energy distributions from 0.060 to 3.3 MeV at 6.6 Earth radii, J. Geophys. Res., **75**(28), 5373−5385, https://doi.org/10.1029/JA075i028p05373, 1970.
Vacaresse, A., Boscher, D., Bourdarie, S., Blanc, M., and Sauvaud, J. A.: Modeling the high-energy proton belt, J. Geophys. Res. Space Phys., **104**(A12), 28601–28613, https://doi.org/10.1029/1999JA900411, 1999.
Venkatesan, D., and Krimigis, S. M.: Observations of low-energy (0.3– to 1.8–MeV) differential spectrums of trapped protons, J. Geophys. Res., **76**(31), 7618–7631, https://doi.org/10.1029/JA076i031p07618, 1971.
Vernov, S. N.: The Earth's radiation belts. In G. Bozóki, E. Gombosi, A. Sebestyén, A. Somogyi (Eds.), Proc. 11th ICRC, Budapest, 85–162, 1969.
Westphalen, H., and Spjeldvik, W.N.: On the energy dependence of the radial diffusion coefficient and spectra of inner radiation belt particles: Analytic solution and comparison with numerical results, J. Geophys. Res., **87**(A10), 8321−8326, https://doi.org/10.1029/2000JA087iA10p08321, 1982.
Wilken, B., Baker, D. N., Higbie, P. R., Fritz, T. A., Olson, W. P., and Pfitzer, K. A.: Magnetospheric configuration and energetic particle effects associated with a SSC: A case study of the CDAW 6 event on March 22, 1979, J. Geophys. Res., **91**(A2), 1459−1473, https://doi.org/10.1029/JA091iA02p01459, 1986.
Williams, D. J.: Phase space variations of near equatorially mirroring ring current ions, J. Geophys. Res., **86**(A1), 189−194, https://doi.org/10.1029/JA086iA01p00189, 1981.
Williams, D. J., and Frank, L. A.: Intense low-energy ion populations at low equatorial altitude, J. Geophys. Res., **89**(A6), 3903−3911, https://doi.org/10.1029/JA089iA06p03903, 1984.

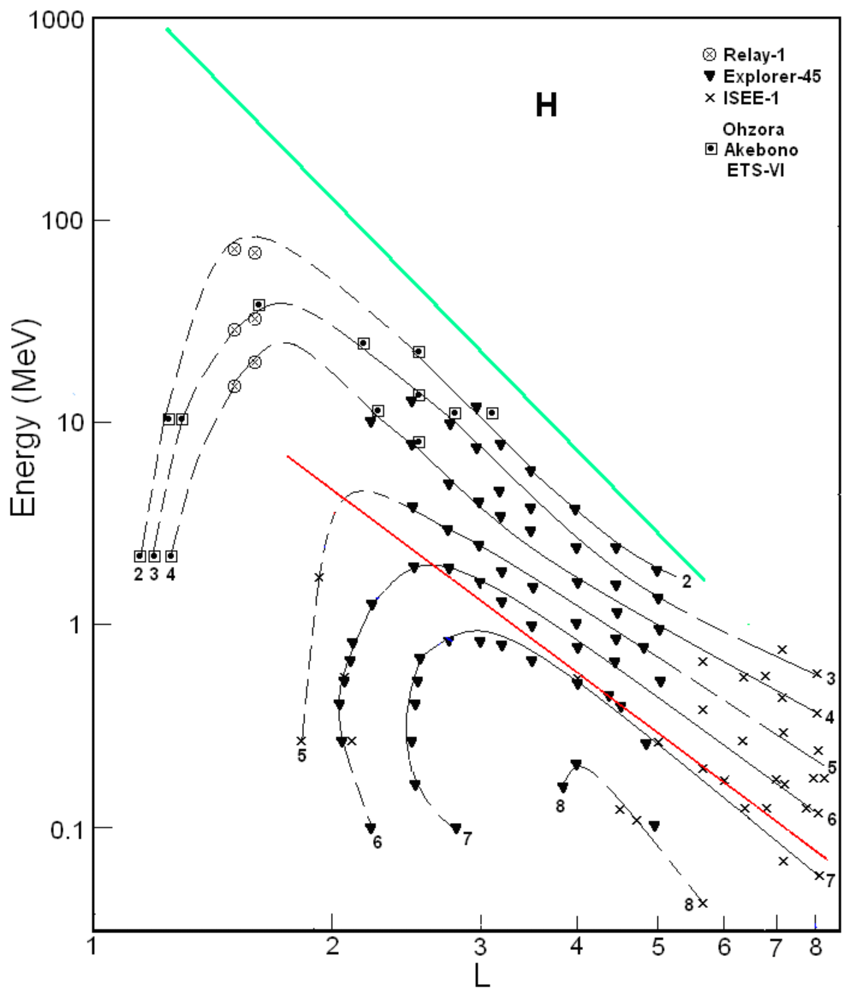

Figure 1. Proton fluxes in the ERB near minima of the solar activity. ~~A~~ The numbers on the curves ~~are equal~~ refer to the values of the decimal logarithms of J where J is given in $(\text{cm}^2\ \text{s ster MeV})^{-1}$ ~~; it~~ is the differential fluxes of protons with $\alpha_0 \approx 90^{o}$ (near the plane of the geomagnetic equator). Data of satellites are ~~presented~~ associated by different symbols. The red line ~~corresponded~~ corresponds to the lower boundary of the power-law tail of the proton spectra; while green line ~~corresponded~~ corresponds to the maximum energy of protons trapped in the ERB (Ilyin et al., 1984).

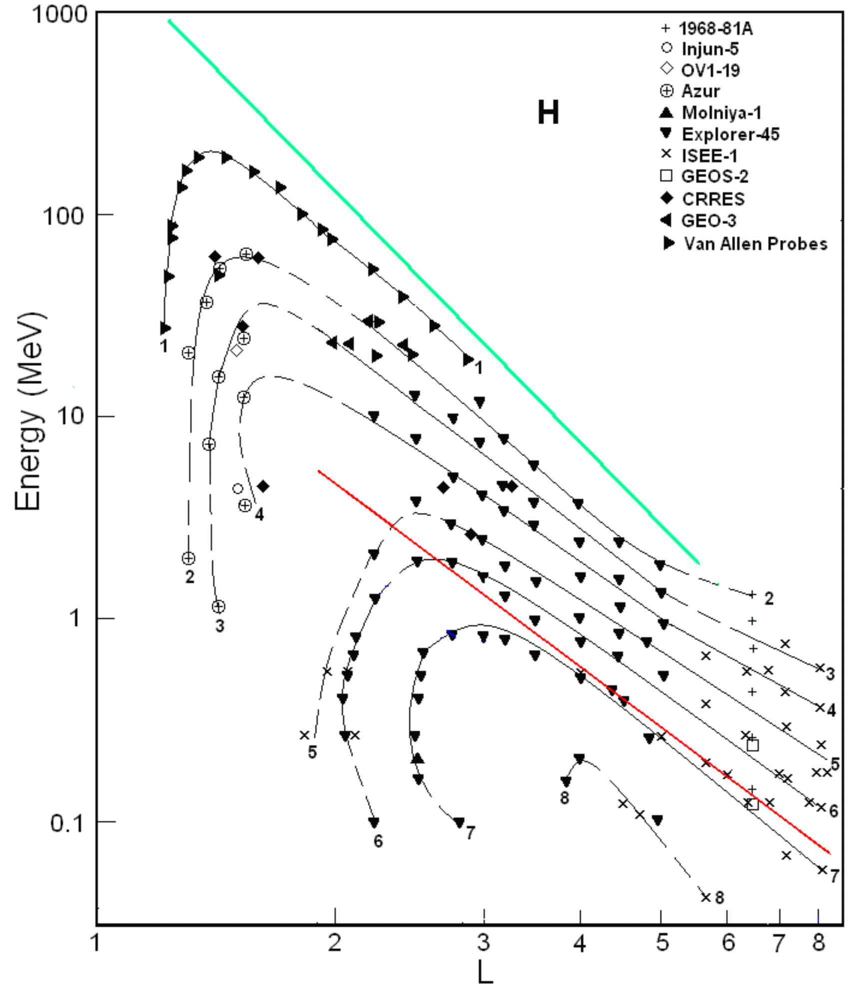

Figure 2. Proton fluxes in the ERB near maxima of the solar activity. The numbers on the curves refer to the values of the decimal logarithms of *J* where *J* is given in $(\mathrm{cm}^2\ \mathrm{s\ ster\ MeV})^{-1}$ is the differential fluxes of protons with $\alpha_0 \approx 90^{\circ}$ (near the plane of the geomagnetic equator). Data of satellites are associated by different symbols. The red line corresponds to the lower boundary of the power-law tail of the proton spectra; while green line corresponds to the maximum energy of protons trapped in the ERB (Ilyin et al., 1984).

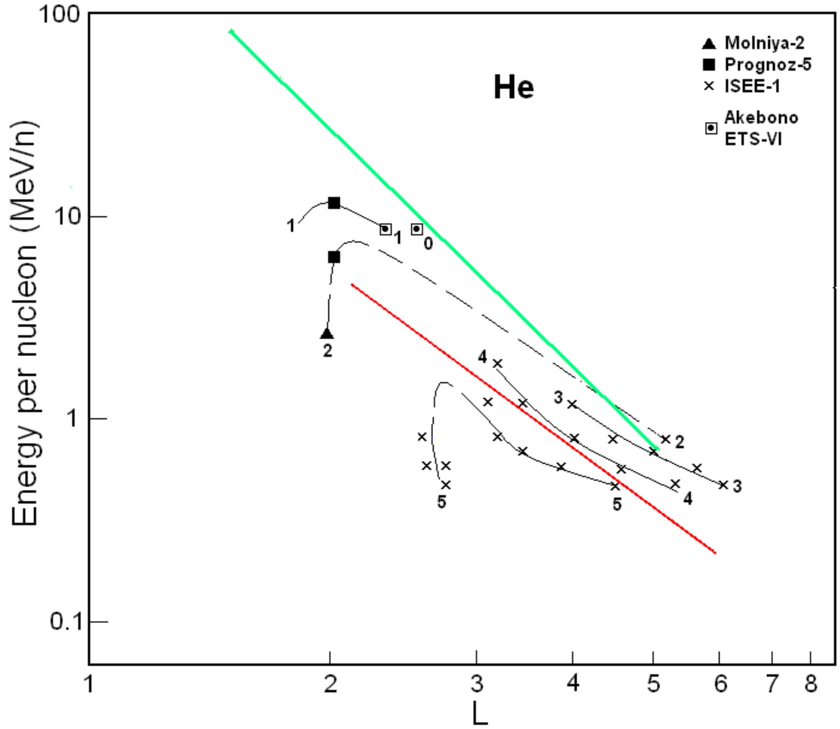

Figure 3. Helium ion fluxes in the ERB near minima of the solar activity. The numbers on the curves refer to the values of the decimal logarithms of *J* where *J* is given in (cm^2 s ster MeV/n)$^{-1}$ is the differential fluxes of helium ions with $\alpha_0 \approx 90^{\circ}$ (near the plane of the geomagnetic equator). Data of satellites are associated by different symbols. The red line corresponds to the lower boundary of the power-law tail of the helium spectra; while green line corresponds to the maximum energy of these ions trapped in the ERB (Ilyin et al., 1984).

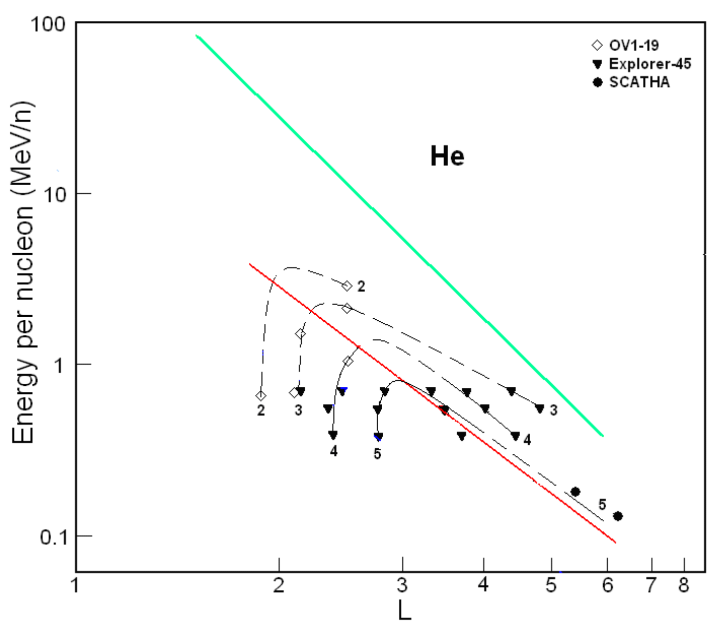

Figure 4. Helium ion fluxes in the ERB near maxima of the solar activity. The numbers on the curves refer to the value of the decimal logarithms of *J* where *J* is given in (cm^2 s ster MeV/n)$^{-1}$ is the differential fluxes of ions with $\alpha_0 \approx 90^{\circ}$ (near the plane of the geomagnetic equator). Data of satellites are associated by different symbols. The red line corresponds to the lower boundary of the power-law tail of the helium spectra; while green line corresponds to the maximum energy of these ions trapped in the ERB (Ilyin et al., 1984).

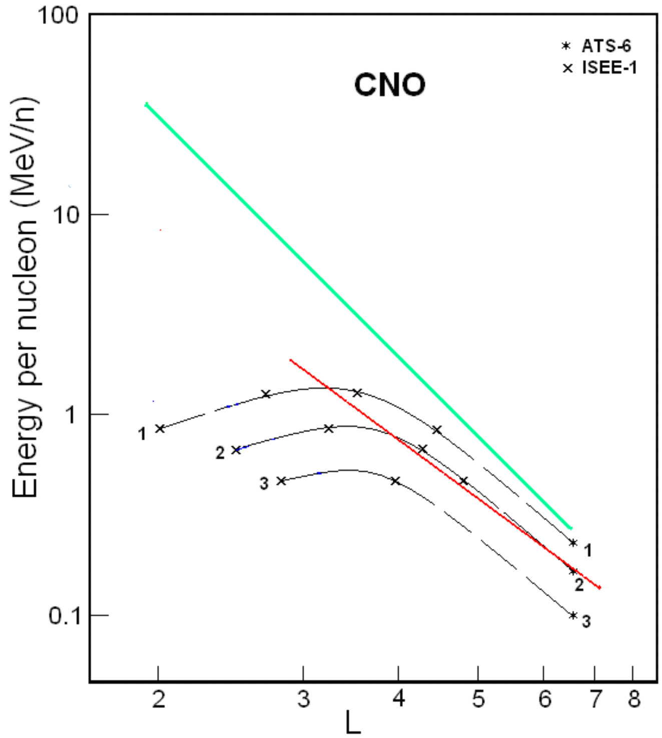

Figure 5. CNO ion fluxes in the ERB near minima of the solar activity. The numbers on the curves refer to the values of the decimal logarithms of J where J is given in (cm^2 s ster MeV/n)$^{-1}$ is the differential fluxes of ions with $\alpha_0 \approx 90^o$ (near the plane of the geomagnetic equator). Data of satellites are associated by different symbols. The red line corresponds to the lower boundary of the power-law tail of the CNO ion spectra; while green line corresponds to the maximum energy of these ions trapped in the ERB (Ilyin et al., 1984).

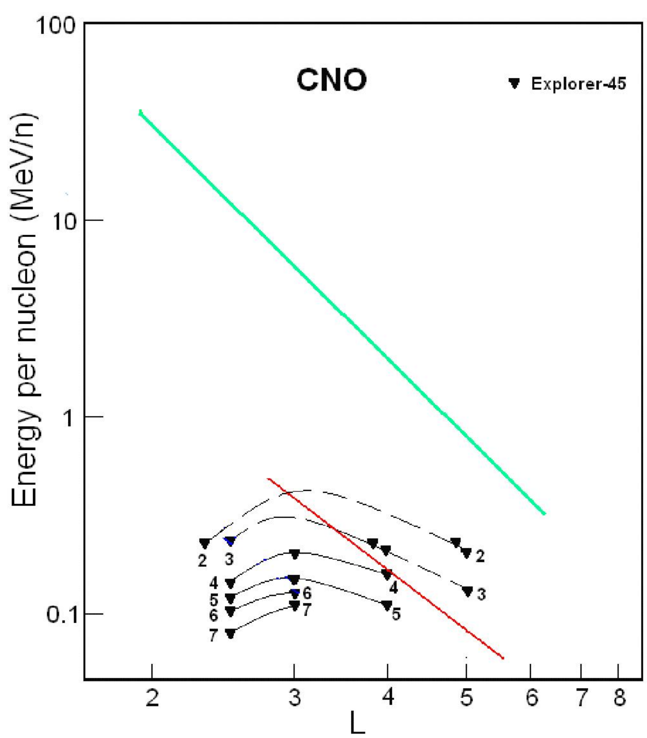

Figure 6. CNO ion fluxes in the ERB near the maximum of the solar activity. The numbers on the curves refer to the values of the decimal logarithms of J where J is given in (cm^2 s ster MeV/n)$^{-1}$ is the differential fluxes of ions with $\alpha_0 \approx 90^o$ (near the plane of the geomagnetic equator). Data of satellites are associated by different symbols. The red line corresponds to the lower boundary of the power-law tail of the CNO ion spectra; while green line corresponds to the maximum energy of these ions trapped in the ERB (Ilyin et al., 1984).